Pertanika J. Sci. & Technol. 33 (2): 969 - 986 (2025)

PERTANIKA JOURNALS

SCIENCE & TECHNOLOGY

Journal homepage: http://www.pertanika.upm.edu.my/

Virus Particle Dispersion and Infection Risk Assessment in Aircraft Cabins: A CFD Approach

Mohd Syakirin Rusdi[1], Di Fey Way[2], Mohd Sharizal Abdul Aziz[1], Farzad Ismail[2] and Mohammad Hafifi Hafiz Ishak[2]*

[1]School of Mechanical Engineering, Universiti Sains Malaysia, Engineering Campus, 14300 Nibong Tebal, Seberang Perai Selatan, Penang, Malaysia
[2]School of Aerospace Engineering, Universiti Sains Malaysia, Engineering Campus, 14300 Nibong Tebal, Seberang Perai Selatan, Penang, Malaysia

ABSTRACT

The work employed computational fluid dynamics to model virus-carrying particle transport mechanisms in a low-cost carrier passenger cabin. The study investigated the effect of virus source location and particle size on particle dynamics and infection risk. The infection risk assessment was conducted based on particle deposition onto surfaces such as passenger bodies and seats. The study found that the direction and velocity magnitude of the airflow in the cabin were almost symmetric about the aisle, with some asymmetry in the velocity magnitude observed due to the coughing passenger's location. Most particles in the cabin were found to be either deposited onto surfaces or removed through the ventilation system within 10 minutes. The study also found that the particle deposition and removal dynamics were strongly affected by the particle source location and the particle size due to the proximity to different surfaces depending on the source location and the propagation distance of the particles, which depends on the gravitational effect based on the size of the particles. The propagation of the particles was found to be mostly contained within the row of the source and two rows in front of the source throughout the 10 minutes. The infection risk assessment indicated a higher risk for passengers seated in the column directly in front of the virus source and for passengers seated on the same side of the aisle as the virus source.

Keywords: Airflow dynamics, computational fluid dynamics (CFD), contaminant transport analysis

ARTICLE INFO

Article history:
Received: 6 August 2024
Accepted: 24 December 2024
Published: 07 March 2025

DOI: https://doi.org/10.47836/pjst.33.2.19

E-mail addresses:
syakirin@usm.my (Mohd Syakirin Rusdi)
dfusm98@gmail.com (Di Fey Way)
msharizal@usm.my (Mohd Sharizal Abdul Aziz)
aefarzad@usm.my (Farzad Ismail)
mhafifihafiz@usm.my (Mohammad Hafifi Hafiz Ishak)
*Corresponding author

INTRODUCTION

Since 2019, the coronavirus disease (COVID-19) has brought about a global pandemic, leading to worldwide health,

ISSN: 0128-7680
e-ISSN: 2231-8526

© Universiti Putra Malaysia Press

safety, and economic crises. The highly infectious COVID-19 was identified to be caused by the severe acute respiratory syndrome coronavirus 2 (SARS-CoV-2), which is the same family of viruses that led to the SARS outbreak between 2002-2004. Initial responses to stop the spread of COVID-19 led to worldwide border restrictions and local movement restrictions. The global economy suffered a huge blow due to these restrictions. The civil aviation industry is one of, if not the most affected sectors globally due to a shortage in international air travel demands. Several studies, including those by Rahman et al. (2020) and Dube (2023), have thoroughly examined the extent of these disruptions. These works underscore the pandemic's unprecedented effects on civil aviation, a sector that continues to grapple with recovery amidst ongoing uncertainties.

The accuracy of Computational Fluid Dynamic (CFD) simulations on particle transport has been validated by comparing them with the results of experimental methods in various studies. For instance, Yan et al. (2009) demonstrated a comparison between experimental and CFD investigation on particle transport mechanisms in a Boeing 767 cabin. They indicated that CFD simulations provided more detailed information that could not be observed or evaluated through experimental setups due to sensor and equipment setup inaccuracy and technological limitations. Zhang et al. (2009) compared experimental and numerical investigations of the airflow and particle transport in a twin-aisle cabin. They concluded that the numerical results of the particle concentration distribution quantitatively agreed with experimental results, but there are some significant differences in the airflow distribution due to the inaccurate measurement of the flow boundary condition from the air supply diffusers. Liu et al. (2013) evaluated the turbulence models in predicting air distribution in aircraft cabins by comparing them with experimental data. They showed that the RNG k-ε, Large eddy simulation (LES) and Detached eddy simulation (DES) turbulence models show satisfactory agreement with the experimental data with small discrepancies in terms of relative accuracy, but the RNG k-ε model was 20 times more efficient in terms of computing time. Q. Wang et al. (2022) evaluated the performance of CFD simulations by comparing the simulation results to actual in-flight transmission studies of 2 long haul flights, including London to Hanoi and Singapore to Hangzhou. They were able to accurately predict 84.2% of the infection in the London to Hanoi flight, and they also found that talking was one of the main methods of spreading COVID-19 in the Singapore to Hangzhou flight. They concluded that face masks are important in preventing the spread of COVID-19 in aircraft passenger cabins.

Multiple studies highlight the significance of seating proximity in SARS-CoV-2 transmission on aircraft. Luo et al. (2023) found that passengers seated within two rows of an infected individual had a higher risk of infection due to short-range airborne transmission, similar to influenza A(H1N1). Schijven et al. (2023) reinforced this, noting that infection risk decreases with distance from the source, supporting the need for measures

like pre-boarding testing and mask-wearing. Aircraft ventilation systems also play a key role. Hui et al. (2023) found that SARS-CoV-2 is less stable on aircraft surfaces, and regular cleaning combined with ventilation effectively reduces transmission. Similarly, Dietrich et al. (2021) showed that vacant middle seats could reduce exposure by up to 57%.

Mask-wearing and surface disinfection further reduce exposure, as Bennett et al. (2022) reported that universal masking decreases exposure by 62% and, combined with distancing, offers greater protection. Additionally, antiviral surface coatings, while effective, require frequent maintenance to remain useful (Hui et al., 2023). Airborne particle behavior in the respiratory system and air filtration are also factors in transmission control (Le Guellec et al., 2023). Khoa et al. (2023) showed how particles deposit in the respiratory tract, which is critical for understanding infection risks. Studies by Lee et al. (2023) and Li et al. (2023) highlighted the role of air filtration in reducing viral loads and particle concentrations, reducing transmission risk. Inhalation is the dominant route of short-range virus transmission, as shown by Chen et al. (2023), emphasizing the importance of ventilation and masking.

Research has long focused on understanding the transmission dynamics of infectious pathogens in enclosed spaces like hospital rooms, classrooms, and aircraft cabins. Morawska et al. (2022) studied respiratory particle behavior and its implications for infection control. Silva et al. (2022) reviewed droplet emission dynamics in public transport, highlighting the role of ventilation and the environment in mitigating airborne infections. Li et al. (2021) conducted an experimental study in a 6-row aircraft cabin mock-up, simulating particle emission from a masked passenger, though these investigations face challenges due to the technical and cost demands.

Most studies focus on long-haul aircraft (e.g., Boeing 700, Airbus A300) because longer flights increase infection risk (Gupta et al., 2020; Chen et al., 2021). However, as global air travel recovers, there is growing demand for short-haul flights, particularly within Europe and Southeast Asia, where low-cost carriers dominate due to affordability and shorter travel times (IATA, 2022). These carriers operate smaller single-aisle aircraft with high passenger density, increasing the risk of airborne infection due to limited social distancing. This underscores the need for studies on virus transmission in low-cost carrier cabins to develop effective mitigation strategies and boost public confidence in air travel.

The primary focus of this study is on understanding how virus source location and particle size affect particle dynamics and the associated infection risk within a low-cost carrier airline cabin. The study modeled particles expelled through coughing and assessed infection risk based on particle deposition on surfaces, including passenger bodies and seats. The research provides insights into how particle size and source location influence the deposition and removal of virus-carrying particles in aircraft cabins.

METHODOLOGY

Physical Model and Computational Domain

The passenger cabin chosen for this study was modeled after the ATR 72-600 aircraft. The cabin geometry was based on dimensions data available from ATR aircraft, as shown in Figure 1. The ATR 72-600 passenger has a standard 72-seat configuration with a 29" (740 mm) seat pitch. This study measured the seat pitch between the back end of the seat headrests. The cabin model only included a single section of the passenger cabin with six rows of seats to reduce the scale of the model and increase computational efficiency.

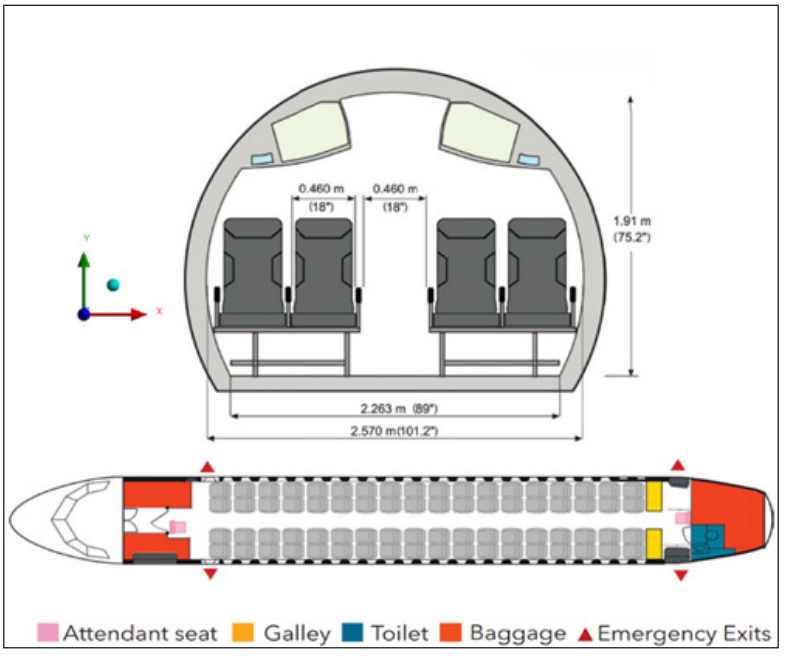

Figure 1. Cross section of ATR 72-600 passenger cabin with dimensions

The cabin interior was modeled according to dimensions available from the ATR aircraft factsheet for the ATR 72-600, as shown in Figure 1. The dimensions of detailed geometry, such as around the stow bins, are modeled by tracing a sketch to scale in Figure 1. The inlet (50mm) and outlet (100mm) of the cabin ventilation system are labeled in yellow and red circles, respectively, in Figure 2. The total length of the cabin was 5 m.

The dimensions of the manikin are modeled by referring to an anthropometric study on Malaysians by Karmegam et al. (2011), which characterized the average dimensions of Malaysians with different ethnicities. The manikin is modeled after the anthropometric data of Chinese females aged 18 to 24 years old. The dimensions of the manikin are summarized in Table 1. The manikin model has an approximate 122 cm seated height with

43 cm shoulder width. A mouth surface is included to be simulated as the source of the expiratory particles. All passengers on board are assumed to have similar dimensions and are always seated in an upright position.

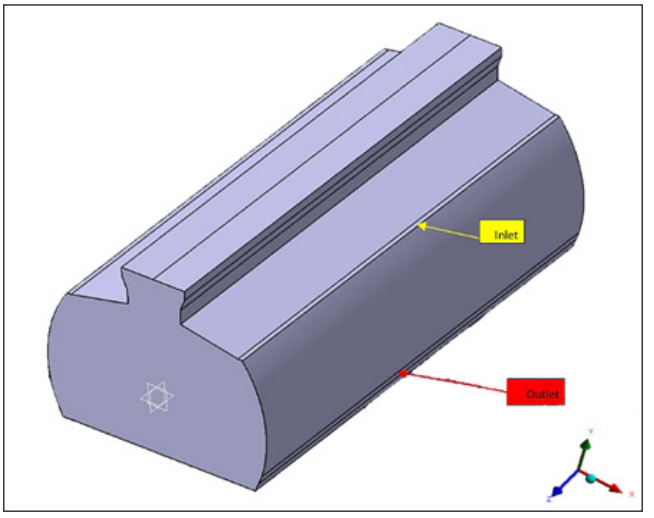

Figure 2. Full Cabin interior solid body

Table 1
Dimensions to model the human manikin (Karmegam et al., 2011)

Anthropometric Component	**Dimensions (mm)**
Head Height	180
Head Width	140
Abdominal Depth	180
Shoulder Height	540
Hand Breadth	70
Elbow Grip Length	336
Thigh Thickness	130
Popliteal Height	393
Buttock Popliteal Length	449
Buttock Knee Length	551

The modeled components are assembled into a 6-row configuration with a 29” (740 mm) seat pitch. The full cabin has four columns of seats with a single aisle in between, which can accommodate 24 passengers. The final assembly is presented in Figure 3. The model assumed full passenger capacity, with all 24 seats filled with passengers seated upright and stationery throughout the study. The seat numbering used in this study is shown in Figure 4.

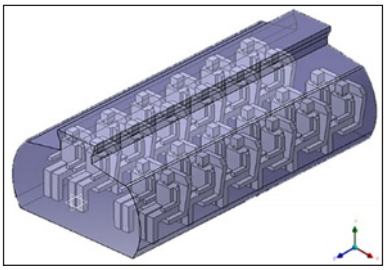

Figure 3. Full cabin assembly

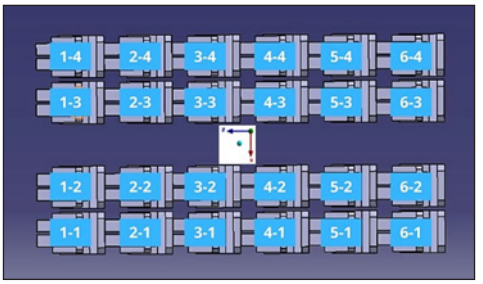

Figure 4. Numbering convention for passenger seat position from the top view

Governing Equations

The flow herein satisfies the incompressible Navier-Stokes (NS) equation with turbulent flow and is solved through the Reynolds-Averaged Navier-Stokes (RANS) equations. Using Einstein's notation in Cartesian coordinates, the continuity is given by Equations 1 and 2.

$$\frac{\partial u_i}{\partial x_i} = 0, \qquad [1]$$

where u_i denotes the fluid velocity in index form. The momentum equation is

$$\frac{\partial (u_i u_j)}{\partial x_j} = -\frac{1}{\rho}\frac{\partial P}{\partial x_i} + g_i + \nu \frac{\partial}{\partial x_j}\left(\frac{\partial u_i}{\partial x_j} + \frac{\partial u_j}{\partial x_i}\right) \qquad [2]$$

where P represents the pressure on the fluids, g_i denotes the gravitational field strength, acting only in the negative y-direction, and the shear stress tensor accounts for the viscous effects on the fluids. The viscosity ν includes physical and eddy viscosities, calculated using the k-ε model.

Turbulence Kinetic Energy, k and Specific Dissipation Rate, ω is given by Equations 3 and 4:

$$\frac{\partial}{\partial t}(\rho k) + \frac{\partial}{\partial x_i}(\rho k u_i) = \frac{\partial}{\partial x_j}\left(\Gamma_k \frac{\partial k}{\partial x_j}\right) + \tilde{G}_k - Y_k + S_k, \qquad [3]$$

$$\frac{\partial}{\partial t}(\rho \omega) + \frac{\partial}{\partial x_i}(\rho \omega u_i) = \frac{\partial}{\partial x_j}\left(\Gamma_\omega \frac{\partial \omega}{\partial x_j}\right) + G_\omega - Y_\omega + D_\omega + S_\omega \qquad [4]$$

where Γ_k and Γ_ω are effective diffusivities of k and ω respectively, $\tilde{G}_k$ is the generation of turbulence kinetic energy due to mean velocity gradients, G_ω is the generation of ω, Y_k and Y_ω are dissipation of k and ω respectively, S_k and S_ω are user-defined source terms, and D_ω is the cross-diffusion term.

The continuous phase solver for turbulence modeling was assumed to be steady-state and pressure-based for incompressible flow. Gravitational acceleration in the negative direction of Y was considered, and the simulation was assumed to be in an isothermal domain, neglecting the effects of heat transfer. The RNG k-ε turbulence model was chosen to model the airflow within the cabin. The suitability of the RNG k-ε turbulence model to predict the airflow in an isothermal cabin was verified by Liu et al. (2013). The working fluid within the domain was air with density (1.1116 kg/m3) and viscosity (1.74645×10-5 kg/m-s).

The air supply for the ventilation system follows recommendations from ASHRAE (2018) for air quality in commercial aircraft. The recommended air supply was 20 cfm per passenger, and for 24 passengers, the total air supply was 480 cfm or approximately 0.2265 m^3/s. Considering the inlet has a surface area of 0.25 m^2, the velocity of the inlet obtained from the air supply flow rate would be 0.9061 m/s. A study examining airflow through ceiling air ventilation in aircraft by Pang et al. (2018) demonstrated that a small angle helped better airflow distribution in confined environments. Furthermore, a study by C. Wang et al. (2022) demonstrated that variations in air supply angles significantly affect airflow distribution in narrow-body aircraft cabins, where small angles (0°–20°) enhance airflow efficiency and passenger comfort. Another study by Talaat et al. (2021), which focuses on airflow in a Boeing 737, found that small angles effectively enhanced airflow and reduced aerosol transmission, supporting the use of smaller angles for optimal performance. Additionally, Shi et al. (2020) examined the impact of air supply positions and angles on cabin thermal comfort, concluding that small angles (5°–30°) improve airflow distribution, particularly for passenger comfort in aircraft cabins. Based on these findings, the 5° angle of the inlet is chosen in accordance with best practices for airflow optimization in regional passenger aircraft. The velocity inlet boundary condition for the ventilation supply was 0.9027 m/s m/s in the horizontal direction of the aisle, respectively, and 0.0790 in the vertical upwards direction.

The mouth surface of the infected passenger also had a velocity inlet boundary of 2.22 m/s, which corresponded to an exhalation of 20 l/min through a 0.00015 m^2 mouth surface. The turbulence intensity and viscosity ratio for the inlet boundaries were left to the default values of 5% and 10%, respectively. The ventilation exhaust was designated an outlet boundary condition with 89 kPa, corresponding to the pressurized cabin at an altitude of approximately 1000 m. Like the inlet boundary, the backflow turbulence intensity and backflow turbulence viscosity ratio for the outlet boundary were also left at 5% and 10%,

respectively. The manikin, seat and cabin wall surfaces were also designated as stationary, with no-slip wall boundary conditions.

Table 2 summarizes the solution methods, including the pressure-velocity coupling scheme and discretization methods. The solver was then initialized using the hybrid method. Lastly, the calculation was run for 2500 iterations until convergence was observed on either the residuals or the outlet velocity monitors.

Table 2
Solution methods in Fluent

Pressure Velocity Coupling	
Scheme	SIMPLE
Gradient	Least Squares Cell-Based
Pressure	Second Order
Momentum	Second Order Upwind
Turbulent Kinetic Energy	Second Order Upwind
Turbulent Dissipation Rate	Second Order Upwind

The discrete phase solver was assumed to be in a transient state, and the discrete phase model with unsteady particle tracking was activated in ANSYS FLUENT v2023. The interaction with the continuous phase option was disabled for a one-way coupling between the continuous and discrete phases. The tracking parameters, including the maximum number of steps and length scale, were specified as 500000 steps and 6 m, respectively.

Monodisperse simulations for different particle sizes were carried out independently because the cubic scaling of spherical particle mass with diameter can affect mass-based distribution when conducting polydisperse particle simulations. Each simulation will have one injection with a uniform particle size, which means four independent simulations with 4 different particle sizes conducted for each seating position case. The particles are assumed to be spherical since the dominant mode for particle transport was momentum diffusivity. The Discrete Random Walk Model is adopted to provide more realistic and diffusive particle trajectories. Particle sizes for each simulation are uniform with 1 μm, 2 μm, 8 μm, and 15.9 μm, respectively. The particle sizes were obtained from the distribution mode size and maximum droplet size determined by Yang et al. (2007) and shown in Table 3.

Lastly, the discrete phase boundary conditions were set up where the inlets and outlets are specified as escape boundary conditions while the walls, including seats, cabin walls, and passenger surfaces, are specified as trap boundary conditions for the deposition of droplets. The particle track will end after the particle has been removed through an escape boundary or deposited on a trap boundary. Finally, the calculation was run for 1200 time steps with a step size of 0.5 seconds, which corresponded to a 10-minute simulation. After the calculation, the particle track data were obtained and extracted for further analysis.

Table 3
Parcel mass and total mass flow rate for each particle size (Yang et al., 2007)

Particle Size (µm)	Parcel Mass (kg)	Total Mass Flow Rate (kg/s)
1	5.235e-16	1.047e-10
2	4.200e-15	8.400e-10
8	2.681e-13	5.632e-8
15.9	2.105e-12	4.209e-7

Grid Independence Test

In this research, Grid Independence Tests (GIT) were used to develop optimal numerical models. The GIT was conducted by solving a simple flow in the cabin by using the RNG k-ε model. The number of mesh elements was increased by decreasing the mesh element size. Two points monitoring the flow velocity located at the outlet are used as reference values for comparison. The hybrid mesh was used to create four different grids. The super fine grid comprises 6.66 million elements, the fine grid has approximately 4.56 million elements, the medium grid contains 3.27 million elements, and the coarse grid includes 1.19 million elements. Figure 5 shows a decreasing trend of flow velocity at outlet velocity reference points as the number of mesh elements increased. Considering the significant increase in the number of mesh elements, from 3.27 million to 6.16 million, the marginal differences between these results were only 6.7% and 3.07 %. However, due to the significant increase in computational time required of approximately 10 hours with less significant results improvement. Therefore, the mesh with 3.27 million elements was selected as the optimal mesh for this study.

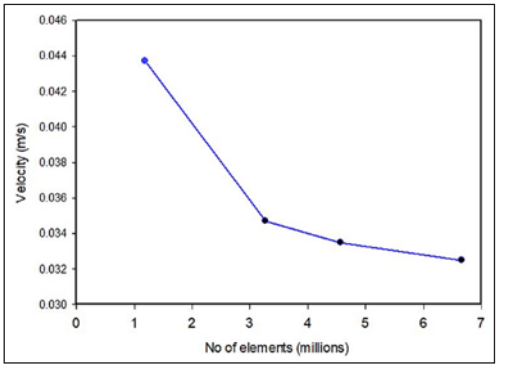

Figure 5. Grid Independence Test Results

CFD Code Validation

It is crucial to compare the current numerical model with previous experimental studies to ensure accurate results. Therefore, a validation study was conducted using the numerical results reported by Talaat et al. (2021), who carried out a similar study in a single-aisle aircraft cabin with three columns of passenger seats. Our study's numerical setup and conditions were identical to those used in the validation to ensure consistency and accuracy. The airflow velocity vector and contour plots from the study are shown in Figure 6. The

vector plot revealed a consistent airflow pattern: air is supplied from the inlet, flows along the cabin walls toward the aisle, and then shifts downward at the aisle section. Further analysis is done by plotting velocity values along the centerline of the cabin, as depicted in Figure 7. The comparison reveals a good agreement between the simulation and experimental data on the front face. There is an average discrepancy of 7.19% between the numerical results reported by Talaat et al. (2021) and current simulation results for velocity contour. These findings indicate the effectiveness of the RANS model in accurately simulating airflow for ventilation phenomena.

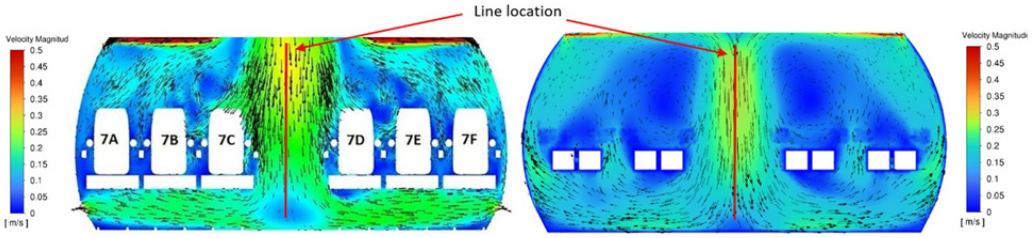

Figure 6. Velocity vector and contour plot. (a) Talaat et al., (2021) and (b) this study

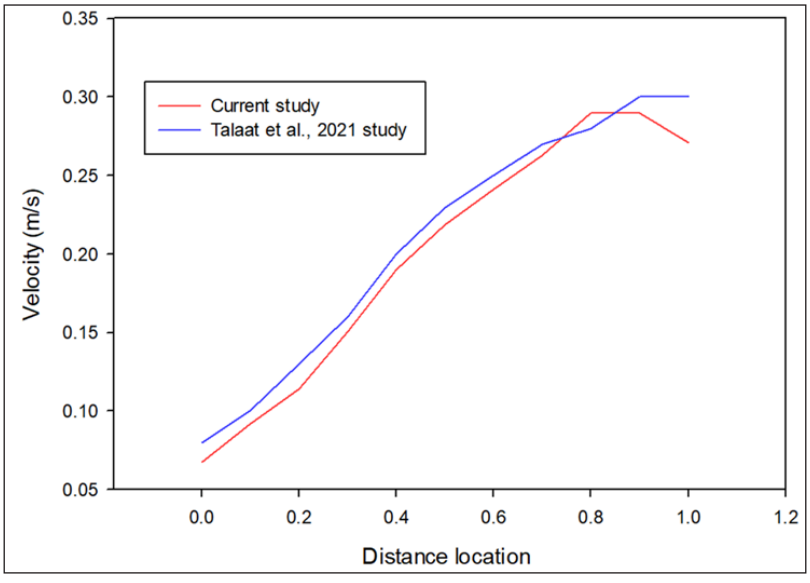

Figure 7. Comparison velocity value along the centerline between Talaat et al. (2021) and this study

RESULTS AND DISCUSSION

The cabin airflow is primarily driven by the ventilation system and influenced by the geometry of passengers, seats, and cabin walls. Figures 8(a) and 8(b) show velocity vectors and contours in the x-y plane for cases where the infected passenger is seated near the aisle

(4-3) and the window (4-4), respectively. In both cases, airflow follows a similar pattern: air enters from the inlet, flows upwards along the upper cabin walls, then moves downwards into the aisle, circulating under the seats toward the exhaust outlets. The downward flow at the aisle splits laterally towards the passenger section, forming a circulation that flows toward the cabin walls without crossing the aisle.

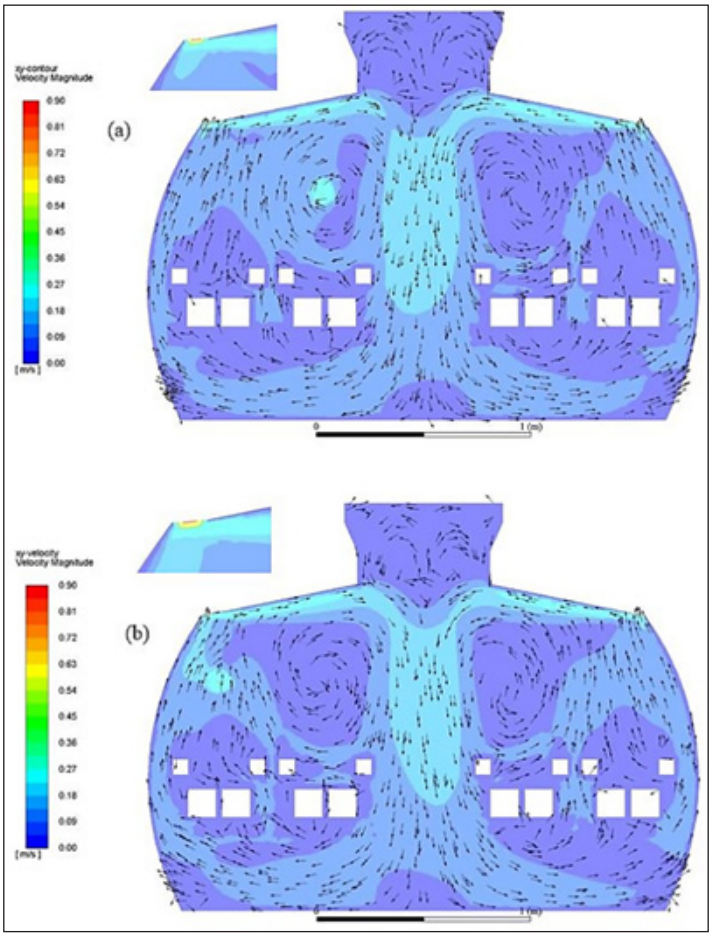

Figure 8. Airflow velocity vector and contour at x-y plane with the infected passenger seated near the (a) aisle (4-3) and (b) window (4-4)

The velocity contours in Figures 8(a) and 8(b) indicate the highest velocity at the ventilation inlet, with velocities decreasing as airflow moves toward the cabin walls, aisle, and exhaust outlets. High-velocity spots depend on the infected passenger's position. Although the velocity distribution is mostly symmetrical, slight asymmetries occur around the passenger section due to different seating positions and the infected passenger exhaling. The overall symmetry results from idealized conditions, assuming uniform passenger geometry and ignoring heat transfer effects on airflow.

Effect Of Infected Passenger Seating Position on Particle Dynamics

The seating position will follow the numbering convention presented in Figure 4. The infected passenger will either be seated near the aisle at seat 4-3 or near the window at seat 4-4. The distribution of 1 μm particles for different infected passenger seats 4-3 and 4-4 with respect to time was presented in Figures 9 and 10, respectively. In 600 seconds, both figures show that the distribution of 1 μm particles is mostly contained within the row of the infected passenger and two rows in front. Both figures also show that after 20 seconds, the particles started to propagate towards the other side of the aisle. At 600 seconds, almost all the particles were either trapped on surfaces or removed through the ventilation system, with only a few particles left trapped within the cabin.

Table 4 highlights the impact of passenger position on particle deposition and removal. Surface deposition is 13.7% higher when particles are released near the aisle (4-3) compared to the window (4-4), while removal is 12.6% higher near the window. Particle depositions on passenger bodies and seats are 3.4% and 27.3% higher near the aisle, but cabin walls show 17% more deposition near the window. Ventilation inlet removal is 15.8% higher near the window, while exhaust outlet removal is 2.1% higher near the aisle. The differences between the particle deposition and removal percentage when released from near the aisle (4-3) and from near the window (4-4) are due to the proximity distance to the surfaces. The

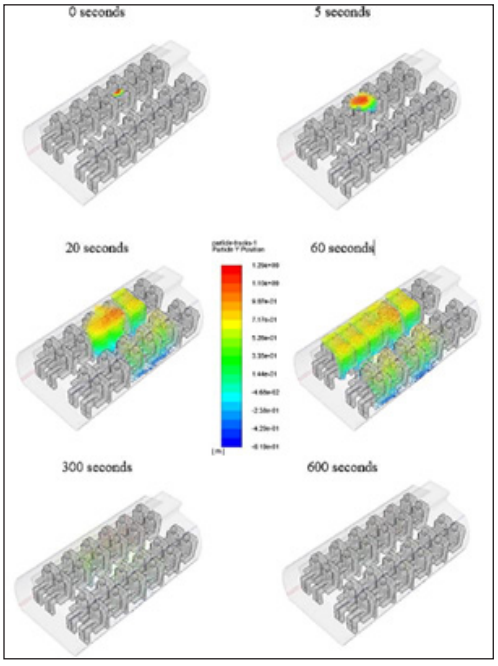

Figure 9. Distribution of 1 μm particles exhaled from seat 4-3 with respect to time

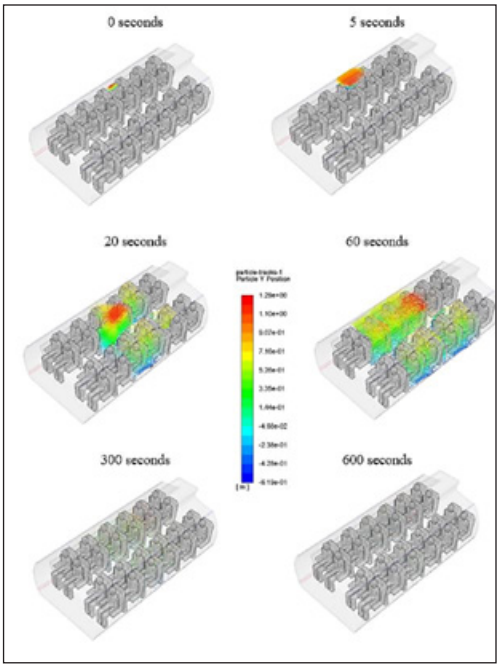

Figure 10. Distribution of 1 μm particles exhaled from seats 4-4 with respect to time

infected passenger seated near the window is much closer to the cabin walls and the inlet than the passenger seated near the aisle. The study by Li et al. (2021) aligns with current findings, which also emphasize the role of seating position and airflow in determining particle deposition and removal. The current study focuses on the effects of seating position near the aisle versus near the window, as well as the detailed quantitative comparison of particle deposition percentages based on these positions. This contributes to a more granular understanding of how different cabin zones and surfaces impact particle behavior.

Table 4
Comparison of particle deposition and removal based on different infected passenger seat positions

Particle Destination		Passenger Seat Position		Difference (%)
		Aisle (4-3)	Window (4-4)	
Deposited (%)	Cabin wall	20.461	37.467	17.006
	Passenger body	31.968	28.584	3.384
	Passenger seats	46.256	18.945	27.311
	Total	98.685	84.996	13.689
Removed (%)	Inlet	5.478	21.234	15.756
	Outlet	6.919	3.776	2.143
	Total	11.397	25.01	12.613

Effect Of Infected Passenger Seating Position on Infection Risk

Particle distribution is mainly confined to the infected passenger's row and the two rows in front. More particles are deposited in the third row (directly in front of the source) than in the fourth row (where the source is). Less deposition occurs on the opposite side of the aisle and back of the source. The aisle seat (4-3) consistently has a higher particle fraction, increasing infection risk, likely due to airflow circulation moving particles toward the cabin walls and reaching 4-3 first. Similar patterns are seen in the second row, with higher deposition at seats 2-3. Overall, infection risk is higher for passengers in front of the source and on the same side of the aisle. The finding is consistent with findings of past studies by To et al. (2009), in which particles expelled by a cough could move forward to the row of seats ahead of the source and lateral air movements influenced the dispersion of these aerosols. This aligns with the result where there was a higher particle deposition on the surfaces in the row directly in front of the particle source.

Effect of Particle Size on Infection Risk

Figure 12 shows the distribution of particle deposition fractions on various seat positions depending on the particle size released from the aisle seat (4- 3). The observations from Figure 12 show an agreement with the observations discussed in Figure 11, where the particle deposition has the highest fraction on the seat directly in front of the source (2-3

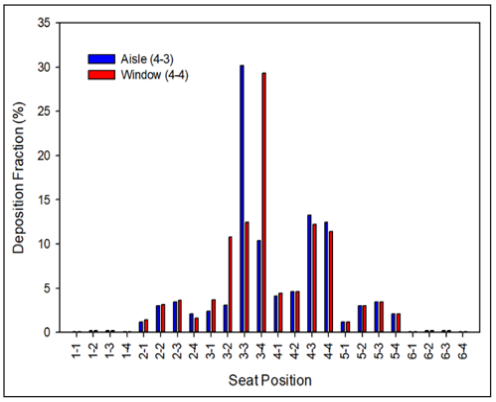

Figure 11. Particle deposition fraction distribution on various seat positions depends on the position of particle release

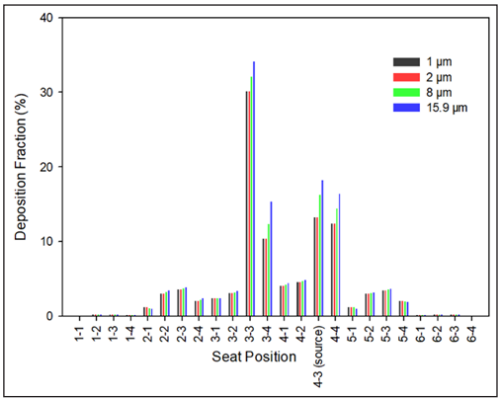

Figure 12. Particle deposition fraction distribution on various seat positions depending on the particle size

and 3-3) and at the location of the source (4-4) compared to other seats of the same row. The deposition is also higher on the same side of the aisle as the source than on the other side of the aisle. As the particle size increases, the deposition fraction also increases at the seat of the particle source (4-3) and the seats directly in front of the source (2-3 and 3-3). On the other hand, the deposition fraction decreases at other seats on the same row as the particle size increases. This could be due to the shorter distance to the surfaces directly in front of the source (2-3 and 3-3) than other lateral seats of the same row. The larger the particle size, the smaller the propagation distance of the particle, resulting in a higher risk of short-range transmission. In summary, the seats directly in front of the source (2-3 and 3-3) and at the source (4-3) have the highest risk of infection, and the risk increases when larger particles are present. Although the risk of infection of passengers seated on other seats of the same row will also increase with the presence of larger particles due to the increase in particle number, the increase of risk is not as high as the seats directly in front of the source (2-3 and 3-3) as there are fewer particles deposited on other seats of the same row compared to the seats directly in front of the source.

Effect of Particle Size on Particle Dynamics

Figure 13 illustrates the correlation between particle size affecting their deposition and removal in an aircraft cabin. Generally, particles are more likely to deposit on surfaces than to be removed via ventilation. Specifically, the highest deposition occurs on passenger seats, followed by passenger bodies and cabin walls. Conversely, the fraction removed through ventilation inlets and outlets is lowest, with larger particles showing a consistent decrease in removal efficiency and an increase in deposition on surfaces. Notably, particles of 8 µm show a slight reduction in seat deposition compared to 1 µm and 15.9 µm particles, likely due to their tendency to be redirected towards cabin walls.

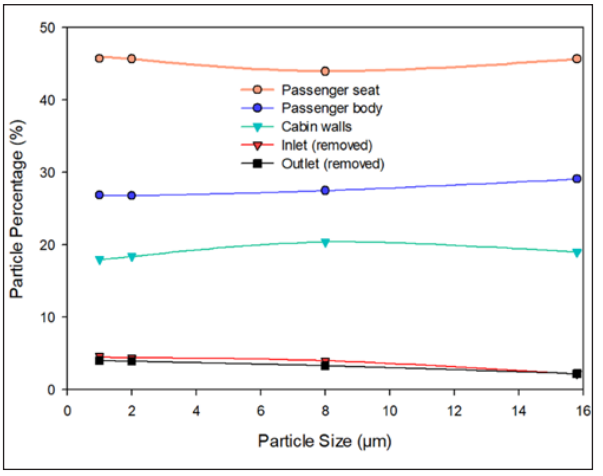

Figure 13. Effect of particle size on particle fate released from aisle seats 4-3

Larger particles have greater mass, enhancing gravitational effects and limiting their travel distance, thus increasing surface deposition risk. This indicates a higher risk of short-range transmission with larger particles. Wang et al. (2011) support these findings, noting that surface deposition exceeds removal through ventilation. These results highlight the importance of tailored cleaning and filtration strategies based on particle size and deposition patterns.

CONCLUSION

The study presented in this paper used computational fluid dynamics (CFD) to investigate virus transmission mechanics in an ATR 72-600 passenger cabin. The results indicated high symmetry in flow directions on both sides of the aisle, with higher velocities near the ventilation inlets, cabin walls, aisle sections, and under seats. The velocity was mostly symmetrical about the aisle, with minor asymmetry near the infected passenger. Particle dynamics, influenced solely by airflow, showed that particle deposition was higher when expelled from the aisle seat compared to the window seat. Surface deposition increases by 13.7% when particles are released near the aisle (4-3) compared to the window (4-4), whereas removal through ventilation is 12.6% higher near the window. Depositions on passenger bodies and seats are 3.4% and 27.3% greater near the aisle, respectively, while deposition on cabin walls is 17% higher near the window. Ventilation inlet removal is 15.8% more effective near the window, whereas exhaust outlet removal is 2.1% higher near the aisle. Conversely, particle removal via the ventilation system was higher for particles released from the window seat. This difference was attributed to the relative proximity of the window seat to cabin walls and ventilation inlets. Particles of 8 μm exhibit a slight

decrease in deposition on seats compared to 1 μm and 15.9 μm particles, likely because they tend to be redirected toward the cabin walls. Larger particles exhibited increased deposition due to gravitational effects, suggesting a higher short-range transmission risk. Based on surface contamination, the infection risk assessment showed a higher risk for seats in front of the infected passenger and on the same side of the aisle. Larger particles increased the infection risk in front of the infected passenger, though the effect was less pronounced for passengers seated in the same row. This study highlights the complex interplay between particle size, seating position, and airflow in determining viral transmission risk in aircraft cabins.

ACKNOWLEDGEMENTS

This work was supported by the Ministry of Higher Education (MoHE) Malaysia for the Fundamental Research Grant Scheme with Project Code: FRGS/1/2022/TK10/USM/03/11

REFERENCES

ASHRAE. (2018). *Air Quality within Commercial Aircraft.* American Society of Heating, Refrigerating and Air-Conditioning Engineers. https://www.ashrae.org/file%20library/technical%20resources/standards%20and%20guidelines/standards%20addenda/161_2018_g_20231130.pdf

Bennett, J., Mahmoud, S., Dietrich, W. L., Jones, B., & Hosni, M. (2022). Evaluating vacant middle seats and masks as Coronavirus exposure reduction strategies in aircraft cabins using particle tracer experiments and computational fluid dynamics simulations. *Engineering Reports, 5*(4), Article e12582. https://doi.org/10.1002/eng2.12582

Chen, Q., Qin, S., & Liu, H. (2021). Airflow and virus transmission in aircraft cabins: CFD simulations and risk analysis. *Building and Environment, 188*, 107-121. https://doi.org/10.1016/j.buildenv.2020.107121

Chen, W., Liu, L., Hang, J., & Li, Y. (2023). Predominance of inhalation route in short-range transmission of respiratory viruses: Investigation based on computational fluid dynamics. In *Building Simulation* (Vol. 16, No. 5, pp. 765-780). Tsinghua University Press. https://doi.org/10.1007/s12273-023-00000-0

Dietrich, W. L., Bennett, J., Jones, B., & Hosni, M. (2021). Laboratory modeling of SARS-CoV-2 exposure reduction through physically distanced seating in aircraft cabins using bacteriophage aerosol. *Morbidity and Mortality Weekly Report, 70*, 595-599. https://doi.org/10.15585/mmwr.mm7016e1

Dube, K. (2023). Emerging from the COVID-19 pandemic: Aviation recovery, challenges, and opportunities. *Aerospace, 10*(1), Article 19. https://doi.org/10.3390/aerospace10010019

Gupta, J. K., Lin, C. H., & Chen, Q. (2020). Risk assessment of airborne infectious diseases in aircraft cabins. *Indoor Air, 21*(1), 3-9. https://doi.org/10.1111/j.1600-0668.2010.00683.x

Hui, K. P., Chin, A., Ehret, J., Ng, K., Peiris, M., Poon, L. L. M., Wong, K. H. M., Chan, M., Hosegood, I., & Nicholls, J. (2023). Stability of SARS-CoV-2 on commercial aircraft interior surfaces with implications for effective control measures. *International Journal of Environmental Research and Public Health, 20*(16), Article 6598. https://doi.org/10.3390/ijerph20166598

IATA. (2022). *Annual Review 2022*. International Air Transport Association. https://www.iata.org/contentassets/c81222d96c9a4e0bb4ff6ced0126f0bb/annual-review-2022.pdf

Karmegam, K., Sapuan, S. M., Ismail, M. Y., Ismail, N., Shamsul Bahri, M. T., Shuib, S., Mohana, G. K., Seetha, P., TamilMoli, P., & Hanapi, M. J. (2011). Anthropometric study among adults of different ethnicity in Malaysia. *International Journal of Physical Sciences, 6*(4), 777–788.

Khoa, N. D., Li, S., Phuong, N. L., Kuga, K., Yabuuchi, H., & Yokota, H. (2023). Computational fluid-particle dynamics modeling of ultrafine to coarse particles deposition in the human respiratory system, down to the terminal bronchiole. *Computer Methods and Programs in Biomedicine, 237*, Article 107589. https://doi.org/10.1016/j.cmpb.2023.107687

Le Guellec, S., Pardessus, J., Bodier-Montagutelli, E., Vecellio, L., de Monte, M., Feteanu, D., Tewes, F., Couet, W., Vecellio, L., & Diot, P. (2023). Administration of bacteriophages via nebulization during mechanical ventilation: *In vitro* study and lung deposition in macaques. *Viruses, 15*(3), Article 602. https://doi.org/10.3390/v15010047

Lee, L. Y. Y., Landry, S. A., Jamriska, M., Subedi, D., McGain, F., & Johnson, G. R. (2023). Quantifying the reduction of airborne infectious viral load using a ventilated patient hood. *Journal of Hospital Infection, 136*, 110-117. https://doi.org/10.1016/j.jhin.2023.103115

Li, L., Pope, Z. C., Son, Y., Eilts, S. M., & Hogan Jr., C. J. (2023). Effects of portable air filtration on submicrometer- and micrometer-sized particle deposition and concentration in a naturally ventilated skilled nursing facility. *Building and Environment, 240*, Article 110454. https://doi.org/10.1016/j.buildenv.2023.109211

Li, X., Zhang, T., Fan, M., Liu, M., Chang, D., Wei, Z., Lin, C. H., Ji, S., Liu, J., Shen, S., & Long, Z. (2021). Experimental evaluation of particle exposure at different seats in a single-aisle aircraft cabin. *Building and Environment, 202*, Article 108049. https://doi.org/10.1016/j.buildenv.2021.108049

Liu, W., Wen, J., Lin, C. H., Liu, J., Long, Z., & Chen, Q. (2013). Evaluation of various categories of turbulence models for predicting air distribution in an airliner cabin. *Building and Environment, 65*, 118–131. https://doi.org/10.1016/j.buildenv.2013.03.023

Luo, Y., Li, Y., Xiao, S., & Lei, H. (2023). Comparative analysis of inflight transmission of SARS-CoV-2, influenza, and SARS-CoV-1. *Epidemiology and Infection, 151*, Article e111. https://doi.org/10.1017/S0950268823001012

Morawska, L., Buonanno, G., Mikszewski, A., & Stabile, L. (2022). The physics of respiratory particle generation, fate in the air, and inhalation. *Nature Reviews Physics, 4*(9), 723-734. https://doi.org/10.1038/s42254-022-00506-7

Pang, Y., Smith, J., & Lee, R. (2018). Optimization of air distribution modes for civil aircraft cabins using CFD. *Journal of Aircraft Engineering and Aerospace Technology, 90*(4), 123-135. https://doi.org/10.1108/JAAET-10-2018-0025

Rahman, N. A. A., Rahim, S. A., Ahmad, M. F., & Hafizuddin-Syah, B. A. M. (2020). Exploring Covid-19 pandemic: Its impact on the global aviation industry and the key strategy. *International Journal of Advanced Science and Technology, 29*(6), 1829–1836.

Schijven, J., van Veen, T., Delmaar, C., Kos, J., Vermeulen, L., Roosien, R., Verhoeven, F., Schipper, M., Peerlings, B., Duizer, E., Derei, J., Lammen, W., Bartels, O., van der Ven, H., Maas, R., & de Roda Husman, A. M. (2023). Quantitative microbial risk assessment of contracting COVID-19 derived from measured and simulated aerosol particle transmission in aircraft cabins. *Environmental Health Perspectives, 131*(8), Article 087011. https://doi.org/10.1289/EHP11495

Shi, X., Chao, D., Zhang, Y., & Zhao, H. (2020). The study of air supply ways effects on the aircraft cabin thermal environment. In R. Wang, Z. Chen, W. Zhang, & Q. Zhu (Eds.), *Proceedings of the 11th International Conference on Modelling, Identification and Control (ICMIC2019)* (Vol. 582, pp. 123-131). Springer. https://doi.org/10.1007/978-981-15-0474-7_12

Silva, P. G., Branco, P. T. B. S., Soares, R. R. G., Mesquita, J. R., & Sousa, S. I. V. (2022). SARS-CoV-2 in indoor environments and the impact of ventilation. *Building and Environment, 219*, Article 109224. https://doi.org/10.1016/j.buildenv.2022.109224

Talaat, K., Abuhegazy, M., Mahfoze, O. A., Anderoglu, O., & Poroseva, S. V. (2021). Simulation of aerosol transmission on a Boeing 737 airplane with intervention measures for COVID-19 mitigation. *Physics of Fluids, 33*(3), Article 033312. https://doi.org/10.1063/5.0040849

To, G. N. S., Wan, M., Chao, C., Fang, L., & Melikov, A. (2009). Experimental study of dispersion and deposition of expiratory aerosols in aircraft cabins and impact on infectious disease transmission. *Aerosol Science and Technology, 43*(5), 466-485. https://doi.org/10.1080/02786820902736658

Wang, C., Zhang, J., Chao, J., Yang, C., & Chen, H. (2022). Evaluation of dynamic airflow structures in a single-aisle aircraft cabin mockup based on numerical simulation. *Indoor and Built Environment, 31*(2), 398–413. https://doi.org/10.1177/1420326X21992094

Wang, Q., Gu, J., & An, T. (2022). The emission and dynamics of droplets from human expiratory activities and COVID-19 transmission in public transport system: A review. *Building and Environment, 219*, Article 109224. https://doi.org/10.1016/j.buildenv.2022.109224

Wang, M., Lin, C. H., & Chen, Q. (2011). Determination of particle deposition in enclosed spaces by detached Eddy simulation with the Lagrangian method. *Atmospheric Environment, 45*(29), 5376-5384. https://doi.org/10.1016/j.atmosenv.2011.06.042

Yan, W., Zhang, Y., Sun, Y., & Li, D. (2009). Experimental and CFD study of unsteady airborne pollutant transport within an aircraft cabin mock-up. *Building and Environment, 44*(1), 34–43. https://doi.org/10.1016/j.buildenv.2008.01.012

Yang, S., Lee, G. W. M., Chen, C. M., Wu, C. C., & Yu, K. P. (2007). The size and concentration of droplets generated by coughing in human subjects. *Journal of Aerosol Medicine: The Official Journal of the International Society for Aerosols in Medicine, 20*(4), 484–494. https://doi.org/10.1089/jam.2007.0610

Zhang, Z., Chen, X., Mazumdar, S., Zhang, T., & Chen, Q. (2009). Experimental and numerical investigation of airflow and contaminant transport in an airliner cabin mockup. *Building and Environment, 44*(1), 85–94. https://doi.org/10.1016/j.buildenv.2008.01.012